Study of a Short Distance Top Mass with a Cross-Section at NNLL + NNLO

by

Brad Bachu

Submitted to the Department of Physics
in partial fulfillment of the requirements for the degree of

Bachelor of Science in Physics

at the

MASSACHUSETTS INSTITUTE OF TECHNOLOGY

June 2017

Author .... Signature redacted .....
Department of Physics
May 12, 2017

Certified by..... Signature redacted .....
Iain W. Stewart
Professor of Physics
Thesis Supervisor

Accepted by ..... Signature redacted ....
Professor Nergis Mavalvala
Physics Associate Head, Department of Physics

Study of a Short Distance Top Mass with a Cross-Section at NNLL + NNLO

by

Brad Bachu

Submitted to the Department of Physics
on May 12, 2017, in partial fulfillment of the
requirements for the degree of
Bachelor of Science in Physics

Abstract

We consider top-quarks produced at large energy in e^+e^- collisions and address the question of what top-mass can be measured from reconstruction. The production process is characterized by the center-of-mass energy, Q, the top mass, m, the top decay width, Γ_t, and also $\Lambda_{\rm QCD}$. These scales are well separated and can be disentangled with effective theory methods such as the Heavy-Quark Effective Theory and Soft-Collinear Effective Theory. We compute a top mass observable for future e^+e^- colliders to next-to-next-to-leading-logarithmic order + $\mathcal{O}(\alpha_s^2)$ (NNLL+NNLO), which goes beyond previous next-to-leading-logarithmic + $\mathcal{O}(\alpha_s)$ (NLL+NLO) analysis. We use the two-loop heavy quark jet-function, $\mathcal{O}(\alpha_s^2)$ corrections to the partonic hemisphere soft function, and hard matching for boosted tops at two loops. We find that the higher order corrections exhibit good convergence and reduced uncertainty in this cross section.

Thesis Supervisor: Iain W. Stewart
Title: Professor of Physics

Acknowledgments

I would like to express my deepest gratitude to Aditya Pathak for inviting me to join this project, and providing continuous guidance and support until its completion. Next, I would like to thank my thesis supervisor Professor Iain Stewart for his helpful discussions and communication throughout the project. Further, I acknowledge Frank Tackmann and Vicent Mateu for their support with SCETlib and cross checks respectively. Lastly, I thank Krishna Rajagopal for advising me throughout my journey as an undergraduate MIT physicists.

Contents

List of Figures

Chapter 1

Introduction

1.1 The Standard Model and the Top Quark

The Standard Model (SM) is currently the simplest model of particle physics which has successfully stood the precision experimental tests performed at particle colliders. It contains fermions which constitute the matter particles, gauge bosons, the force carrier particles, and the scalar Higgs boson that is responsible for giving mass to a majority of the particles. The fermions are categorized into leptons and quarks. There are six leptons and quarks, organized in three generations, with every generation consisting of successively heavier particles (with the possible exception of the neutrinos).

The top quark is not only the heaviest quark, but it is also the heaviest of all the known elementary particles in Standard Model (SM). Its existence was predicted in 1973 by Makoto Kobayashi and Toshihide Maskawa to explain the observed CP violations in kaon decay [1]. The top quark was the last quark to be discovered of all the six and was first observed in 1995 at the CDF and D0 experiments at Fermilab, leading to Kobayashi and Maskawa receiving the Nobel prize in 2008 [2–4]. Today, experimentalists still continue to study properties of the top quark produced at the CMS and ATLAS experiments at the LHC, CERN.

Interest in top phenomenology is driven mainly because of its large mass. It has a mass m_{top} of about 173 GeV, and weighs roughly the same as a gold nucleus. In fact,

the next heaviest quark is its weak isodoublet partner, the bottom quark, weighing in at much smaller mass of 4.2 GeV [5]. The large mass of the top quark can also be understood in terms of Yukawa coupling to the Higgs boson being of $\mathcal{O}(1)$ [5]. As a result, it provides a means to not only constrain SM physics, but also plays an important role in many new physics (NP) searches. A precision top mass determination is important for precision electroweak measurements, constraining extensions to the standard model like supersymmetry, and determination of the stability of the electroweak vacuum (which put in another words determines the 'fate of our universe') [6, 7].

The top quark, like other quarks in second and third generations, is unstable through weak interactions. The top has a large decay width $\Gamma_t = 1.4$ GeV. Since quarks interact strongly they bind into hadrons, a process called confinement. The scale of confinement Λ_{QCD} is about the mass of proton ~ 1 GeV. Since $\Gamma_t > \Lambda_{\text{QCD}}$ the top quark decays before it hadronizes, unlike other quarks which decay after they bind into a hadron. It decays through weak interaction into a real W boson and a down type quark [5], almost entirely $t \to Wb$. The W boson can in turn decay semileptonically into a lepton and a neutrino, or hadronically into two lighter quarks. This unique property of top quark plays a very important role in collider phenomenology. For example, the case of a boosted top, where W decays hadronically, we observe three-prong substructure which can be isolated using jet substructure techniques, such as N-subjettiness [8, 9]. An example of this event is shown in Fig. 1-1. The semileptonic decays requires one to look for a bottom quark, or b-jet, and a lepton in the same event [10, 11] and such decays are useful for tagging top-events.

1.2 Top Quark Mass Measurements

The current combined measurement of the top mass from the Tevatron and LHC is $173.34 \pm 0.27(\text{stat}) \pm 0.71(\text{syst})$ GeV [12]. Measurement of m_{top} can be broadly classified into two main categories: direct and indirect determinations of m_{top}.

Indirect determinations of m_{top} are based on the comparison of total or differential

$t\bar{t}$ production cross-section to the corresponding theory calculations. Indirect determinations have the advantage in that they allow direct comparison between theory and experiment, and a clearer theoretical interpretation of the measured m_{top} [13], however they have significantly larger experimental uncertainties.

Direct m_{top} measurements exploit information from the kinematic reconstruction of top-quark decay products [13]. Examples include the 'template method' [2, 3], 'matrix element method' [14], and the 'ideogram method' [15].

Direct measurements are the most precise and natural methods for top mass determination. However, problems arise because its mass is a priori not directly observable, as the top is a parton carrying non-vanishing color charge. In fact, the top mass should be considered as a renormalization scheme-dependent coupling in the quantum chromodynamics (QCD) Lagrangian rather than a physical object, just like the strong coupling α_s [16]. Moreover, since the top mass is not a unique physical quantity, the reconstruction method and prescription also affects the mass obtained. Measured top masses are assumed to be measurements of the pole mass, and the relation between Monte Carlo generator mass and the pole is uncertain at the level of 1GeV [17], which is now comparable to the measurement uncertainty [5].

A main goal of our study of kinematically sensitive top cross-sections directly from QCD, rather than Monte Carlo, is to eliminate this uncertainty. In this context certain top quark mass renormaliation schemes are more suitable for precision measurements than others since the choice of scheme can affect the higher order behavior of the perturbative corrections as well as the organization of power corrections. Suitable quark mass schemes are compatible with the power counting and also lead to an optimal behavior of the perturbative expansion. Such schemes can be identified and defined unambiguously if the precise relation of the observable to a given Lagrangian top quark mass scheme can be established. For finite order perturbative calculations the choice of the scheme can impact the accuracy of the mass measurement, and amongst various commonly used schemes only a class of schemes called 'short distance schemes' are suitable As a result, it is useful to study an observable which allows us to extract top-mass in a precisely defined short distance scheme.

There does exists a well studied systematic analytic framework where the measured top mass and the Lagrangian top mass parameter m can be related: A threshold scan of the line-shape of the total hadronic cross section in the top-antitop threshold region, $Q \approx 2m$ at a future Linear Collider, where Q is the c.m. energy [18–20]. Unfortunately, this cannot be applied at the LHC. This is because the threshold scan uses the rise of the line-shape of the cross section near a center of mass energy that is related to a toponium-like top-antitop bound state [21–23], and at the LHC, the top anti-top invariant mass cannot be determined with a relative uncertainty sufficient enough to resolve the top-antitop threshold region [24].

1.3 Problem Statement

With the absence of a threshold scan, our current goal is to measure m_t at the LHC, which is a proton proton (pp) collider. To begin with, as protons are composite objects, not only is there more radiation in the beam than in e^- collisions, there is also added complexity from the parton density functions (PDFs), that determine the fraction of quarks and gluons in a proton. Additional complications at the LHC include radiation induced from multi-parton-interactions (MPI's), and pileup that occurs because we are colliding bunches of protons. These measurements necessarily involve jets and hence depend on the choice of jet definition and parameters like the jet radius. In this thesis, we study the simpler scenario of an $e^+e^- \to$ top-jets, which allows us to study some issues in great detail with high precision, while postponing other issues to the eventual extension to the $pp \to$ top-jets case. The e^+e^- results can also be used to calibrate Monte Carlo programs which are then applied to pp [25].

Through the use of Effective Field Theories (EFTs) it is possible it devise observables which satisfy certain factorization properties that allow us to extract a top mass while satisfying the constraints of having a kinematic sensitivity and control of the top mass scheme. The production of top quarks at high energies in e^+e^- collisions is characterized by well separated scales such as the center-of-mass energy, Q, the top mass, m, the top decay width, Γ_t, and also $\Lambda_{\rm QCD}$, in the following manner:

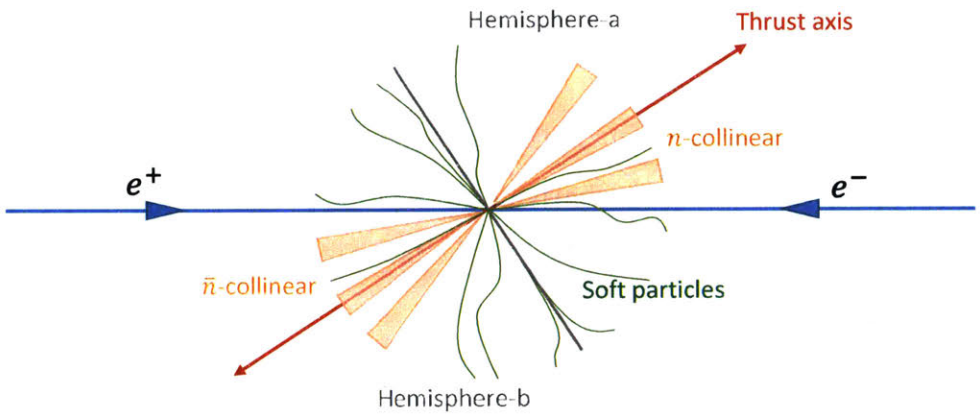

Figure 1-1: Six jet event initiated by a top quark pair, $t\bar{t} \to bW\bar{b}W \to bqq'\bar{b}qq'$. The plane separating the two hemispheres is perpendicular to the thrust axis and intersects the thrust axis at the interaction point. The total invariant mass inside each hemisphere is measured. We do not consider leptonic decays of top here.

$Q \gg m \gg \Gamma_t > \Lambda_{\rm QCD}$. The appropriate EFT for this problem is the Soft Collinear Effective Theory (SCET) [26, 27]. SCET is an effective theory that describes the interactions of soft and collinear degrees of freedom in the presence of a hard interaction. It describes QCD in the infrared, but allows for both soft homogeneous and collinear inhomogeneous momenta for the particles [26, 27].

In Ref. [16], it was proposed that the kinematic measurement of the double differential invariant hemisphere mass distribution, $\left(\frac{d\sigma}{dM_t^2 dM_{\bar{t}}^2}\right)$, in the peak region around top resonance, provides an event shape which is sensitive to the top mass and also a framework to yield the mass in a definite scheme. In Refs. [16, 28], this has been computed and discussed in detail. Following the prescription set out in Refs. [16, 28], we consider boosted tops so that its decay products will be in one hemisphere. In Fig. 1-1, we show a sketch of such an event. We treat the evolution and decay of the top close to mass shell using Boosted Heavy Quark Effective Theories (bHQET) [29] for the interactions of the heavy quark with the soft degrees of freedom.

In this thesis, we compute a top mass observable for future e^+e^- colliders to NNLL+NNLO (next-to-next-to-leading-logarithmic order + $O(\alpha_s^2)$), which goes beyond the NLL+NLO analysis in Ref. [28]. We will use the two-loop heavy quark

jet-function in the heavy quark limit and the relations of the jet-mass to the pole and $\overline{\text{MS}}$ at two-loop order [30]. We will include $\mathcal{O}(\alpha_s^2)$ corrections to the partonic hemisphere soft function that sums large logarithmic terms, $\frac{Q}{m_t}$ and $\frac{m_t}{\hat{s}}$ (where $\hat{s} = \frac{M_t^2 - m_t^2}{m_t}$ encodes the measurement and m_t is the short-distance top quark mass) and separates perturbative from nonperturbative effects [31–34]. These are ingredients that still need to be systematically combined in the factorized cross-section, and this nontrivial task is the goal of this thesis.

In Section 2, we present the factorization theorem along with its ingredients that allow us to compute the cross section to NNLL+NNLO. In Section 3, we describe how these ingredients are combined mathematically, and then discuss the implementation method in Section 4. In Section 5, we summarize the results.

Chapter 2

The Cross Section

We calculate the double differential invariant hemisphere mass distribution $\frac{\mathrm{d}\sigma}{\mathrm{d}M_t^2\,\mathrm{d}M_{\bar{t}}^2}$. In Ref. [28], it was shown that at leading order in the expansion in $\frac{m}{Q}$ and $\frac{\Gamma}{m}$ this distribution can be factorized into the form

$$\begin{aligned}\frac{\mathrm{d}\sigma}{\mathrm{d}M_t^2\,\mathrm{d}M_{\bar{t}}^2} &= \sigma_0 H_Q\left(Q,\mu\right) H_m\left(m,\frac{Q}{m},\mu\right) \\ &\times \int \mathrm{d}l^+\,\mathrm{d}l^- B_+\left(\hat{s}_t - \frac{Ql^+}{m},\Gamma,\delta m,\mu\right) B_-\left(\hat{s}_{\bar{t}} - \frac{Ql^-}{m},\Gamma,\delta m,\mu\right) \\ &\times S_{\mathrm{hemi}}(l^+,l^-,\mu)\,, \end{aligned} \tag{2.1}$$

where:

1. $M_{t,\bar{t}}^2$ are the invariant masses defined from all particles in each of the two hemispheres that are determined by the plane perpendicular to the event's thrust axis.

2. σ_0 is a normalization factor, referred to as the tree level Born cross section.

3. $Q \sim 0.5 - 1\mathrm{TeV}$ is the center of mass energy of the e^+e^- collision

4. m is the Lagrangian top mass parameter in a chosen scheme, $m = m^{\mathrm{scheme}}$.

5. $\delta m = m^{\mathrm{pole}} - m^{\mathrm{scheme}}$. Perturbative corrections that depend on the choice of

the scheme which are encoded by the difference to the pole mass

$$\delta m(R,\mu) = \sum_{n=1}^{\infty} \left(\frac{\alpha_s(\mu)}{4\pi}\right)^n \delta m_i = R \sum_{n=1}^{\infty} \sum_{k=0}^{n} a_{nk} \left[\frac{\alpha_s(\mu)}{4\pi}\right]^n \ln^k\left(\frac{\mu}{R}\right), \quad (2.2)$$

where R is a dimension 1 parameter that specifies as an infrared (IR) cut off related to the scheme, and a_{nk} are scheme dependent numbers.

6. H_Q and H_m, known as the hard functions, are matching corrections that are derived from matching between QCD and SCET at Q, and SCET and bHQET at m, respectively. H_Q and $H_m$are independent of $\hat{s}_t$ and $\hat{s}_{\bar{t}}$ and do not affect the form of the invariant mass distribution, but only act as normalization factors.

7. $\hat{s}_{t,\bar{t}} \equiv \frac{s_{t,\bar{t}}}{m} \equiv \frac{M^2_{t,\bar{t}} - m^2}{m} \sim \Gamma \ll m$, shifted variables introduced for convenience, as it is only the invariant mass distribution close to the peak we wish to predict. This is also the most sensitive region for mass measurements in the peak region.

8. The jet functions $B_{\pm}(\hat{s}, \Gamma, \delta m, \mu)$ describe the QCD dynamics of collinear radiation in the top/antitop direction, and the decay of the top and antitop quarks near mass shell within the top/antitop jets. They can be computed perturbatively at the scale $\mu \gtrsim \Gamma$ since the top width Γ provides an infrared cutoff from hadronization. At tree level, they are simply Breit-Wigner (BW) functions:

$$B_{\pm}(\hat{s}, \Gamma, \delta m, \mu) = \frac{1}{\pi m} \frac{\Gamma}{\hat{s}^2 + \Gamma^2} + \mathcal{O}(\alpha_s) \quad (2.3)$$

where the ellipses indicate QCD corrections that distort the BW. Further, we can express the bHQET jet function for the physical unstable top $B_{\pm}(\hat{s}, \Gamma, \delta m, \mu)$ as a convolution of the stable jet function $B_{\pm}(\hat{s}, \Gamma = 0, \delta m, \mu)$ with a BW function of width Γ [28],

$$B_{\pm}(\hat{s}, \Gamma, \delta m, \mu) = \int_{-\infty}^{\hat{s}} \mathrm{d}\hat{s}' B_{\pm}(\hat{s} - \hat{s}', \Gamma = 0, \delta m, \mu) \frac{\Gamma}{\pi(\hat{s}'^2 + \Gamma^2)} \quad (2.4)$$

Note that the upper limit $\hat{s}$ of integration can be replaced by $+\infty$ since the stable jet function only has support for positive values of its energy variable.

We use the two-loop heavy quark jet-function in the heavy quark limit computed in Ref. [30].

9. The soft function $S_{\rm hemi}(l^+, l^-, \mu)$ describes the physics of the soft perturbative and nonperturbative gluons through which the top and antitop jets can communicate. The partonic part, $S_{\rm part}$, of the hemisphere soft function $S_{\rm hemi}$ can be computed in perturbation theory at scale $\mu_\Lambda \geq \Lambda_{\rm QCD}$. We account for the nonperturbative corrections from hadronization using a model function F. We first observe that the corrections are enhanced in the peak region, as compared to the tail region. This feature can be realized by modeling the soft function as [35],

$$S_{\rm hemi}(l^+, l^-, \mu) = \int_{-\infty}^{+\infty} \mathrm{d}\bar{l}^+ \int_{-\infty}^{+\infty} \mathrm{d}\bar{l}^- S_{\rm part}(l^+ - \bar{l}^+, l^- - \bar{l}^-, \mu) \times F(\bar{l}^+ - \Delta, \bar{l}^- - \Delta)\,, \tag{2.5}$$

where the parameters of F can be determined from experimental data. Furthermore, we have included a gap parameter Δ to account for minimum hadronic deposit in each hemisphere.

Additionally, we can define unitary evolution functions U_i, for the various hard, jet and soft functions. For example, the renormalization group evolution for the jet function is given by

$$B_\pm(\hat{s}, \Gamma, \delta m, \mu) = \int \mathrm{d}\hat{s}' U_{B_\pm}(\hat{s} - \hat{s}', \mu, \mu_\Gamma) B_\pm(\hat{s}', \Gamma, \delta m, \mu_\Gamma)\,. \tag{2.6}$$

This equation allows us to express $B_\pm$ at its natural scale $\mu_\Gamma \sim \hat{s} \sim \Gamma$. Substituting Eq. (2.5), and Eq. (2.4) into our factorization theorem Eq. (2.1), and using evolution

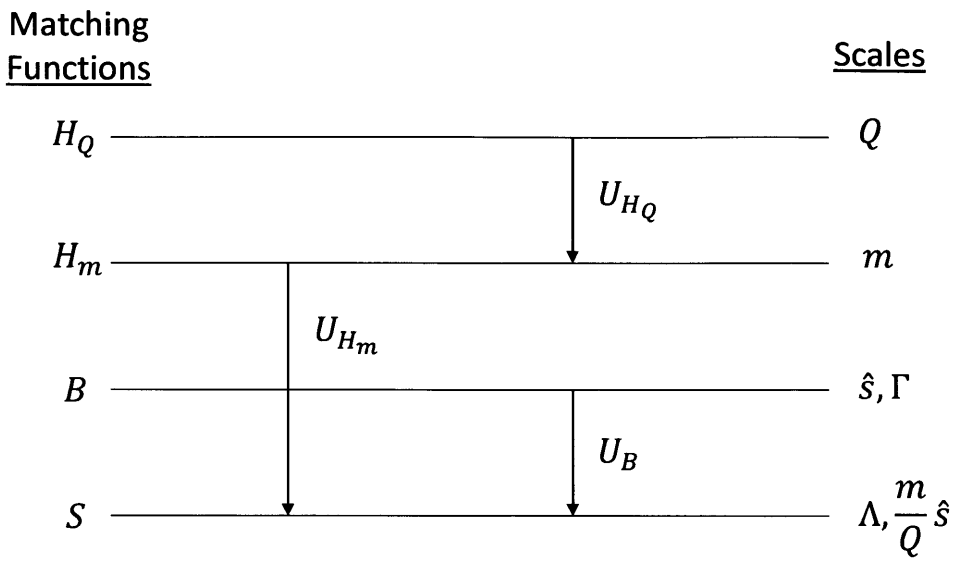

Figure 2-1: Scales together with the corresponding matching and evolution functions appearing in the formula for the invariant mass distribution.

equations like Eq. (2.6) we obtain,

$$\begin{aligned}\frac{\mathrm{d}\sigma}{\mathrm{d}M_t^2\,\mathrm{d}M_{\bar{t}}^2} &= \sigma_0 H_Q\left(Q,\mu_Q\right) U_{H_Q}(Q,\mu_Q,\mu_m) H_m\left(m,\frac{Q}{m},\mu_m\right) U_{H_m}\left(\frac{Q}{m},\mu_m,\mu_\Lambda\right)\\ &\times\int \mathrm{d}l^+\int \mathrm{d}l^-\int \mathrm{d}\hat{s}_t'\int \mathrm{d}\hat{s}_{\bar{t}}' U_B\left(\hat{s}_t-\hat{s}_t',\mu_\Gamma,\mu_\Lambda\right) U_B\left(\hat{s}_{\bar{t}}-\hat{s}_{\bar{t}}',\mu_\Gamma,\mu_\Lambda\right)\\ &\times\int \mathrm{d}\hat{s}_t''\int \mathrm{d}\hat{s}_{\bar{t}}'' B_+\left(\hat{s}_t'-\frac{Ql^+}{m}-\hat{s}_t'',\Gamma_t=0,\mu_\Gamma\right) B_-\left(\hat{s}_{\bar{t}}'-\frac{Ql^-}{m}-\hat{s}_{\bar{t}}'',\Gamma_{\bar{t}}=0,\mu_\Gamma\right)\\ &\times\int \mathrm{d}\tilde{l}^+\,\mathrm{d}\tilde{l}^- S_{\mathrm{part}}(l^+-\tilde{l}^+,l^--\tilde{l}^-,\mu) F(\tilde{l}^+,\tilde{l}^-)\frac{\Gamma_{\bar{t}}}{\pi(\hat{s}_{\bar{t}}''+\Gamma_{\bar{t}}^2)}\frac{\Gamma_t}{\pi(\hat{s}_t''+\Gamma_t^2)}\,. \end{aligned} \tag{2.7}$$

In the rest of this section, we give explicit representations of the hard functions H_Q and H_m, the stable jet functions $B_\pm$, the partonic soft function S_{part} as well as the model function F.

2.1 Common Definitions

We provide a list of definitions that appear in the following sections:

1. $C_A = N_c = 3$ is the adjoint Casmir of QCD.

2. $C_F \equiv \frac{N_c^2-1}{2N_c} = \frac{4}{3}$ is the fundamental Casmir of QCD.

3. $T_F = \frac{1}{2}$, appearing from a trace of QCD color generators $tr[T^A T^B] = T_F \delta^{AB}$

4. n_l is the number of light quarks.

5. ζ_n is the Riemann zeta function or Euler Riemann zeta function defined as $\zeta_n = \zeta(n) = \sum_{m=1}^{\infty} \frac{1}{m^n}$.

6. $\Gamma^0 = 4C_F$ cusp anomolous dimension at one-loop order. Γ^i = loop at $i+1$ loop order

7. γ^0 noncusp anomolous dimension at one-loop order. γ^i = loop at $i+1$ loop order.

8. $\gamma^E \approx 0.577$ is the Euler-Mascheroni constant.

9. $\beta_0 = \frac{11}{3}C_A - \frac{4}{3}n_f T_F$, is the one loop β-function coefficient, where n_f is the number of active quarks (which is often equal to n_l).

2.2 The Hard Functions

We obtain the hard function H_Q from the relation with the Wilson coefficient via

$$H_Q = |C_Q|^2 . \tag{2.8}$$

In the following, we abbreviate the appearing logarithms as

$$L_m = \log\left(\frac{m^2}{\mu^2}\right), \qquad L_Q = \ln\left(\frac{-Q^2 - i0}{\mu^2}\right).$$

The two-loop expression for C_Q, widely used in the SCET literature, and obtained with the aid of the massless form factor calculation of Refs. [36,37], is given by

$$
\begin{aligned}
C_Q^{(n_l+1)} = 1 &+ \frac{\alpha_s^{(n_l+1)}(\mu) C_F}{4\pi} \left\{ - L_Q^2 + 3L_Q - 8 + \frac{\pi^2}{6} \right\} \\
&+ \left(\frac{\alpha_s^{(n_l+1)}(\mu)}{4\pi} \right)^2 C_F^2 \left\{ \frac{1}{2} L_Q^4 - 3L_Q^3 + \left(\frac{25}{2} - \frac{\pi^2}{6} \right) L_Q^2 - \left(\frac{45}{2} + \frac{3\pi^2}{2} - 24\zeta_3 \right) L_Q \right. \\
&\qquad \left. + \frac{255}{8} + \frac{7\pi^2}{2} - 30\zeta_3 - \frac{83\pi^4}{360} \right\} \\
&+ \left(\frac{\alpha_s^{(n_l+1)}(\mu)}{4\pi} \right)^2 C_A C_F \left\{ \frac{11}{9} L_Q^3 - \left(\frac{233}{18} - \frac{\pi^2}{3} \right) L_Q^2 + \left(\frac{2545}{54} + \frac{11\pi^2}{9} - 26\zeta_3 \right) L_Q \right. \\
&\qquad \left. - \frac{51157}{648} - \frac{337\pi^2}{108} + \frac{313\zeta_3}{9} + \frac{11\pi^4}{45} \right\} \\
&+ \left(\frac{\alpha_s^{(n_l+1)}(\mu)}{4\pi} \right)^2 C_F T_F (n_l + 1) \left\{ - \frac{4}{9} L_Q^3 + \frac{38}{9} L_Q^2 - \left(\frac{418}{27} + \frac{4\pi^2}{9} \right) L_Q \right. \\
&\qquad \left. + \frac{4085}{162} + \frac{23\pi^2}{27} + \frac{4\zeta_3}{9} \right\} . \qquad (2.9)
\end{aligned}
$$

The hard function H_m in the n_l-flavor scheme with the top-mass in the pole scheme $\left(\alpha_s^{(n_l)} \equiv \alpha_s^{(n_l)}(\mu)\right)$ [38], is given by

$$
\begin{aligned}
H_m^{(n_l)}\left(m, \frac{q}{m}, \mu\right) = 1 &+ \frac{\alpha_a^{(n_l)}(\mu)}{4\pi} C_F \left(2L_m^2 - 2L_m + 8 + \frac{\pi^2}{3}\right) \\
&+ \left(\frac{\alpha_s^{(n_l)}(\mu)}{4\pi}\right)^2 C_F^2 \left\{2L_m^4 - 4L_m^3 + \left(18 + \frac{2\pi^2}{3}\right) L_m^2 - \left(19 - \frac{10\pi^2}{3} + 48\zeta_3\right) L_m \right. \\
&\qquad \left. + \frac{305}{4} + 10\pi^2 - 16\pi^2 \log 2 - 12\zeta_3 - \frac{79\pi^4}{90}\right\} \\
&+ \left(\frac{\alpha_s^{(n_l)}(\mu)}{4\pi}\right)^2 C_A C_F \left\{-\frac{22}{9} L_m^3 + \left(\frac{167}{9} - \frac{2\pi^2}{3}\right) L_m^2 - \left(\frac{1165}{27} + \frac{56\pi^2}{9} - 60\zeta_3\right) L_m \right. \\
&\qquad \left. + \frac{12877}{324} + \frac{323\pi^2}{54} + 8\pi^2 \log 2 + \frac{178\zeta_3}{9} - \frac{47\pi^4}{90}\right\} \\
&+ \left(\frac{\alpha_s^{(n_l)}(\mu)}{4\pi}\right)^2 C_F n_l T_F \left\{\frac{8}{9} L_m^3 - \frac{52}{9} L_m^2 + \left(\frac{308}{27} + \frac{16\pi^2}{9}\right) L_m - \frac{1541}{81} - \frac{74\pi^2}{27} - \frac{104\zeta_3}{9}\right\} \\
&+ \left(\frac{\alpha_s^{(n_l)}(\mu)}{4\pi}\right)^2 C_F T_F \left\{ - \frac{16}{9} L_m^3 - \frac{4}{9} L_m^2 + \left(\frac{260}{27} + \frac{4\pi^2}{3}\right) L_m + \frac{5106}{81} - \frac{82\pi^2}{27} - \frac{8\zeta_3}{9} \right. \\
&\qquad \left. - \left(\frac{8}{3} L_m^2 + \frac{80}{9} L_m + \frac{224}{27}\right) \log\left(\frac{Q^2}{m^2}\right) \right\}. \qquad (2.10)
\end{aligned}
$$

2.3 The Heavy Quark Jet Function

The stable heavy quark jet function for a (fictitious) top quark having zero width was computed in of Ref. [30] at two loop order:

$$
\begin{aligned}
mB(\hat{s},\delta m,\mu) = \delta(\hat{s}) + \frac{C_F\alpha_s(\mu)}{\pi}\left\{2\,\mathcal{L}^1_{\hat{s}} - \mathcal{L}^0_{\hat{s}} + \left(1-\frac{\pi^2}{8}\right)\delta(\hat{s})\right\} - \frac{2\alpha_s(\mu)}{\pi}\delta m_1(\mu)\delta'(\hat{s}) \\
+ \frac{\alpha_s^2(\mu)}{\pi^2}\Bigg\{C_F^2\left[2\,\mathcal{L}^3_{\hat{s}} - 3\,\mathcal{L}^2_{\hat{s}} + \left(3-\frac{11\pi^2}{12}\right)\mathcal{L}^1_{\hat{s}} + \left(-1+\frac{11\pi^2}{24}+4\zeta_3\right)\mathcal{L}^0_{\hat{s}}\right. \\
\left. + \left(\frac{1}{2}-\frac{5\pi^2}{24}+\frac{13\pi^4}{57600}-2\zeta_3\right)\delta(\hat{s})\right] \\
+ C_F C_A\left[\left(\frac{2}{3}-\frac{\pi^2}{6}\right)\mathcal{L}^1_{\hat{s}} + \left(-\frac{5}{18}+\frac{\pi^2}{12}+\frac{5\zeta_3}{4}\right)\mathcal{L}^0_{\hat{s}}\right. \\
\left. + \left(-\frac{11}{54}-\frac{\pi^2}{144}+\frac{23\pi^4}{2880}-\frac{5\zeta_3}{8}\right)\delta(\hat{s})\right] \\
+ C_F\beta_0\left[-\frac{1}{2}\,\mathcal{L}^2_{\hat{s}} + \frac{4}{3}\,\mathcal{L}^1_{\hat{s}} + \left(-\frac{47}{36}+\frac{\pi^2}{12}\right)\mathcal{L}^0_{\hat{s}} + \left(\frac{281}{216}-\frac{59\pi^2}{576}-\frac{17\zeta_3}{48}\right)\delta(\hat{s})\right]\Bigg\} \\
- \frac{2\alpha_s^2(\mu)}{\pi^2}\left\{\delta m_2\delta'(\hat{s}) - (\delta m_1)^2\delta''(\hat{s}) + \delta m_1 C_F\left[2(\mathcal{L}^1_{\hat{s}})' - (\mathcal{L}^0_{\hat{s}})' + \left(1-\frac{\pi^2}{8}\right)\delta'(\hat{s})\right]\right\}.
\end{aligned}
\tag{2.11}
$$

where we refer to A.1 for the definition of the log plus-functions $\mathcal{L}^n_{\hat{s}}$. To be consistent, we use the notation for the plus functions $\mathcal{L}_n(\hat{s})$ defined in Appendix B of Ref [39] as

$$
\mathcal{L}_n(\hat{x}) = \left[\frac{\theta(\hat{x})\ln^n\hat{x}}{\hat{x}}\right]_+ . \tag{2.12}
$$

The $\mathcal{L}^n_{\hat{s}}$ in Eq. (2.11) is related to $\mathcal{L}_n(\hat{s})$ of Eq. [2.12] by

$$
\mathcal{L}^n_{\hat{s}} \equiv \frac{1}{\mu}\left[\frac{\theta(\hat{s})\ln^k(\hat{s}/\mu)}{\hat{s}/\mu}\right]_+ = \frac{1}{\mu}\,\mathcal{L}_n\left(\frac{\hat{s}}{\mu}\right). \tag{2.13}
$$

2.4 The Partonic Soft Function

In Eq. (2.5) the convolution transfers the gap to give $l^{\pm} > \Delta$. This allows for an hadronic interpretation for these variables. However, in perturbation theory there is a

renormalon ambiguity of $\mathcal{O}(\Lambda_{\rm QCD})$ at the partonic threshold. Following Ref. [31,35], we remove the renormalon contributions in the partonic soft function by explicit subtractions. This can be achieved by writing

$$\Delta = \bar{\Delta} + \delta\bar{\Delta}\,, \tag{2.14}$$

where $\delta\bar{\Delta}$ is a perturbative series in α_s

$$\delta\bar{\Delta} = \delta\bar{\Delta}_1 + \delta\bar{\Delta}_2 + \delta\bar{\Delta}_3 + \ldots\,, \tag{2.15}$$

that contains exactly the same $\mathcal{O}(\Lambda_{\rm QCD})$ renormalon as the soft function. Eq. (2.5) for the soft function now can be expressed as

$$\begin{aligned} S_{\rm hemi}(l^+, l^-, \mu) = \int_{-\infty}^{+\infty} {\rm d}\bar{l}^+ \int_{-\infty}^{+\infty} {\rm d}\bar{l}^- S_{\rm part}(l^+ - \bar{l}^+ - \delta\bar{\Delta}, l^- - \bar{l}^- - \delta\bar{\Delta}, \mu) \\ \times F(\bar{l}^+ - \bar{\Delta}, \bar{l}^- - \bar{\Delta})\,. \end{aligned} \tag{2.16}$$

To cancel the renormalon between the partonic soft function and the series $\delta\bar{\Delta}$ order-by-order in α_s expansion we now have to expand Eq. (2.5) in the $\delta\bar{\Delta}_i$ simultaneously with the expansion for the partonic soft function $S_{\rm part} = S^0_{\rm part} + S^1_{\rm part} + S^1_{\rm part} + ...$, so that

$$\begin{aligned} S_{\rm part}(l^\pm - \delta\bar{\Delta}, \mu) = S^0_{\rm part}(l^\pm, \mu) + \left[S^1_{\rm part}(l^\pm, \mu) - \delta\bar{\Delta}_1 \left(\frac{\rm d}{{\rm d}l^+} + \frac{\rm d}{{\rm d}l^-}\right) S_{\rm part}(l^\pm, \mu)\right] \\ + \left[S^2_{\rm part}(l^\pm, \mu) - \left(\frac{\rm d}{{\rm d}l^+} + \frac{\rm d}{{\rm d}l^-}\right) \left\{\delta\bar{\Delta}_2 S^0_{\rm part}(l^\pm, \mu) + \delta\bar{\Delta}_1 S^1_{\rm part}(l^\pm, \mu)\right\}\right] \\ + \left(\frac{{\rm d}^2}{{\rm d}l^{+2}} + \frac{{\rm d}^2}{{\rm d}l^{-2}} + 2\frac{{\rm d}^2}{{\rm d}l^+\,{\rm d}l^-}\right) \frac{\delta\bar{\Delta}_1^2}{2} S^0_{\rm part}(l\pm, \mu)\,, \end{aligned} \tag{2.17}$$

where $\delta\bar{\Delta}_i$ and $S^i_{\rm part}$ are of order $\mathcal{O}(\alpha_s^i)$, and $\delta\bar{\Delta}_1$ and $\delta\bar{\Delta}_2$ are defined as [$L_{\mu R} \equiv \ln(\mu/R), \alpha_s = \alpha_s(\mu)$],

$$\delta\bar{\Delta}_1(R,\mu) = \left(\frac{\alpha_s}{4\pi}\right)\left[\gamma_s^0 + 2\Gamma_s^0 L_{\mu R}\right] = \left(\frac{\alpha_s}{4\pi}\right)\left[-8C_F L_{\mu R}\right] Re^{\gamma_E}\,,$$
$$\delta\bar{\Delta}_2(R,\mu) = \left(\frac{\alpha_s}{4\pi}\right)^2\left[2t_1\beta_0 + \gamma_s^1 + 2\left(\beta_0\gamma_0 + \Gamma_s^1\right)L_{\mu R} + 2\beta_0\Gamma_s^0 L_{\mu R}^2\right)\Big] Re^{\gamma_E}\,.$$

The partonic soft function, $S_{\rm part}$, in momentum space is defined as [31],

$$\begin{aligned}
S_{\rm part}(l^+,l^-,\mu) &= \delta(l^+)\delta(l^-) \\
&+ \left(\frac{C_F\alpha_s}{4\pi}\right)\left\{\left[-8\,\mathcal{L}_+^1 + \frac{\pi^2}{6}\delta(l^+)\right]\delta(l^-) + \left[-8\,\mathcal{L}_-^1 + \frac{\pi^2}{6}\delta(l^-)\right]\delta(l^+)\right\} \\
&+ \left(\frac{\alpha_s}{4\pi}\right)^2\left\{C_F^2\left[-8\,\mathcal{L}_+^1 + \frac{\pi^2}{6}\delta(l^+)\right]\left[-8\,\mathcal{L}_-^1 + \frac{\pi^2}{6}\delta(l^-)\right] + 32C_F^2\left[\delta(l^+)\,\mathcal{L}_-^3 + \delta(l^-)\,\mathcal{L}_+^3\right]\right. \\
&\quad + \left[\frac{88}{3}C_A C_F - \frac{32}{3}C_F T n_f\right]\left[\delta(l^+)\,\mathcal{L}_-^2 + \delta(l^-)\,\mathcal{L}_+^2\right] \\
&\quad + \left[-12\pi^2 C_F^2 + C_A C_F\left(-\frac{536}{9} + \frac{8}{3}\pi^2\right) + \frac{160}{9}C_F T n_f\right]\left[\delta(l^+)\,\mathcal{L}_-^1 + \delta(l^-)\,\mathcal{L}_+^1\right] \\
&\quad + \left[64\zeta_3 C_F^2 + C_A C_F\left(\frac{808}{27} - \frac{22}{9}\pi^2 - 28\zeta_3\right) + C_F T n_f\left(-\frac{224}{27} + \frac{8}{9}\pi^2\right)\right] \\
&\qquad \times\left[\delta(l^+)\,\mathcal{L}_-^0 + \delta(l^-)\,\mathcal{L}_+^0\right] \\
&\quad + \left[-\frac{3}{40}\pi^4 C_F^2 + C_A C_F\left(\frac{134}{27}\pi^2 - \frac{2}{9}\pi^4 + \frac{176}{9}\zeta_3\right) + C_F T n_f\left(-\frac{40}{27}\pi^2 - \frac{64}{9}\zeta_3\right)\right] \\
&\qquad \left.\times 2\delta(l^+)\delta(l^-) + 2t_2(l^+,l^-)\right\}, \qquad (2.18)
\end{aligned}$$

where

$$\mathcal{L}_\pm^n \equiv \frac{1}{\mu}\left[\theta(l^\pm)\frac{\ln^n(l^\pm/\mu)}{(l^\pm/\mu)}\right]_+ . \qquad (2.19)$$

To be consistent, again we have that $\mathcal{L}_\pm^n$ in Eq. (2.18) is related to $\mathcal{L}_n$ of Eq. (2.12) by

$$\mathcal{L}_\pm^n \equiv \frac{1}{\mu}\left[\theta(l^\pm)\frac{\ln^n(l^\pm/\mu)}{(l^\pm/\mu)}\right]_+ = \frac{1}{\mu}\mathcal{L}_n\left(\frac{l^\pm}{\mu}\right). \qquad (2.20)$$

$t_2(l^+,l^-)$ in Eq. (2.18) represents the non-global part of the soft function and is calculated in Ref. [32]. We give an approximate formula for t_2 in Eq. (3.14) below.

2.5 The Model Function

Following Ref. [39], the model function is implemented as follows:

$$F(l^+, l^-) = \sum_{i,j=0}^{\infty} \frac{c_{i,j}}{\Lambda^2} f_i\left(\frac{l^+}{\Lambda}\right) f_j\left(\frac{l^-}{\Lambda}\right), \tag{2.21}$$

where Λ is a dimension 1 parameter that specifies the scale of the nonperturbative corrections and are fixed such that they are normalized. The f_n's above are defined as follows:

$$f_n(x) = 8\sqrt{\frac{2x^3(2n+1)}{3}} e^{-2x} P_n\left[y(x,3)\right], \tag{2.22}$$

where

$$y(x,3) = 1 - 2\left(1 + 4x + 8x^2 + \frac{32}{3}x^3\right) e^{-4x}, \tag{2.23}$$

Here $f_n(x)$ are a complete set of orthonormal functions,

$$\int_0^{\infty} \mathrm{d}x f_m(x) f_n(x) = \delta_{mn}, \tag{2.24}$$

and $P_n(y)$ are the normalized Legendre polynomials

$$P_n(y) = \frac{1}{2^n n!} \frac{\mathrm{d}^n}{\mathrm{d}y^n} (y^2 - 1)^n. \tag{2.25}$$

Eq. (2.21) is completely general with the coefficient's $c_{i,j}$ specifying the model to be used. In practice the sum on i and j are truncated and the basis has been chosen so that the first few terms provide an accurate description of functions whose large $l^{\pm}$ is governed by confinement.

Chapter 3

Computing the Cross Section

In Chapter 2, we showed that the cross section can be factorized as,

$$\begin{aligned}\frac{\mathrm{d}\sigma}{\mathrm{d}M_t^2\,\mathrm{d}M_{\bar{t}}^2} &= \sigma_0 H_Q\left(Q,\mu_Q\right) U_{H_Q}(Q,\mu_Q,\mu_m) H_m\left(m,\frac{Q}{m},\mu_m\right) U_{H_m}\left(\frac{Q}{m},\mu_m,\mu_\Lambda\right)\\ &\times \int \mathrm{d}l^+ \int \mathrm{d}l^- \int \mathrm{d}\hat{s}_t' \int \mathrm{d}\hat{s}_{\bar{t}}' U_B\left(\hat{s}_t-\hat{s}_t',\mu_\Gamma,\mu_\Lambda\right) U_B\left(\hat{s}_{\bar{t}}-\hat{s}_{\bar{t}}',\mu_\Gamma,\mu_\Lambda\right)\\ &\times \int \mathrm{d}\hat{s}_t'' \int \mathrm{d}\hat{s}_{\bar{t}}'' B_+\left(\hat{s}_t'-\frac{Ql^+}{m}-\hat{s}_t'',\Gamma_t=0,\mu_\Gamma\right) B_-\left(\hat{s}_{\bar{t}}'-\frac{Ql^-}{m}-\hat{s}_{\bar{t}}'',\Gamma_{\bar{t}}=0,\mu_\Gamma\right)\\ &\times \int \mathrm{d}\tilde{l}^+\,\mathrm{d}\tilde{l}^- S_{\mathrm{part}}(l^+-\tilde{l}^+,l^--\tilde{l}^-,\mu) F(\tilde{l}^+,\tilde{l}^-)\frac{\Gamma_{\bar{t}}}{\pi(\hat{s}_{\bar{t}}''+\Gamma_{\bar{t}}^2)}\frac{\Gamma_t}{\pi(\hat{s}_t''+\Gamma_t^2)}\,. \end{aligned} \tag{3.1}$$

Combining all the terms above and carrying out the integrals represent the main task of this thesis. In this section, we outline the computation procedure used.

3.1 Combining perturbative Jet and Soft Functions

From the formula above we see that the σ_0 and the hard functions only affect the normalization. The shape of the differential cross section is determined by the jet and soft function. These functions involve non trivial plus distributions. The focus of this section is to combine plus distributions in both B and S and turn them into analytic

G_n functions, defined later. Thus, we restrict ourselves to the following integral,

$$\begin{aligned}\frac{\mathrm{d}\sigma^{\mathrm{part}}}{\mathrm{d}M_t^2\,\mathrm{d}M_{\bar{t}}^2} \propto & \int \mathrm{d}l^+ \int \mathrm{d}l^- \int \mathrm{d}\hat{s}_t' \int \mathrm{d}\hat{s}_{\bar{t}}' U_B\left(\hat{s}_t - \hat{s}_t', \mu_\Gamma, \mu_\Lambda\right) U_B\left(\hat{s}_{\bar{t}} - \hat{s}_{\bar{t}}', \mu_\Gamma, \mu_\Lambda\right) \\ & \times \int \mathrm{d}\hat{s}_t'' \int \mathrm{d}\hat{s}_{\bar{t}}'' B_+\left(\hat{s}_t' - \frac{Ql^+}{m} - \hat{s}_t'', \Gamma_t = 0, \mu_\Gamma\right) B_-\left(\hat{s}_{\bar{t}}' - \frac{Ql^-}{m} - \hat{s}_{\bar{t}}'', \Gamma_{\bar{t}} = 0, \mu_\Gamma\right) \\ & \times S_{\mathrm{part}}(l^+, l^-, \mu) \frac{\Gamma_{\bar{t}}}{\pi(\hat{s}_{\bar{t}}''^2 + \Gamma_{\bar{t}}^2)} \frac{\Gamma_t}{\pi(\hat{s}_t''^2 + \Gamma_t^2)} \,. \end{aligned} \tag{3.2}$$

3.1.1 Combining Plus Distributions

We see that B contains $\frac{1}{\mu_\Gamma}\mathcal{L}_n\left(\frac{\hat{s}'-\hat{s}''-\frac{Q}{m}l}{\mu_\Gamma}\right)$ and S_{part} contains $\frac{1}{\mu_\Lambda}\mathcal{L}_n\left(\frac{l^\pm}{\mu_\Lambda}\right)$. Hence, the product above contains convolution of plus distributions of the form:

$$\int \mathrm{d}l^+ \frac{1}{\mu_\Gamma}\mathcal{L}_n\left(\frac{\hat{s}' - \frac{Ql^+}{m} - \hat{s}_t''}{\mu_\Gamma}\right) \frac{1}{\mu_\Lambda}\mathcal{L}_m\left(\frac{l^+}{\mu_\Lambda}\right) \,. \tag{3.3}$$

The plus distributions can be combined by either using convolution identities or by going to the position space. Note that these functions are at different scales and it is easier to combine them when they are at the same scale. Hence, we define a change of variables $\frac{Q}{m}l^\pm = \hat{s}^\pm$, and then apply the following rescaling identity ($\lambda > 0$),

$$\lambda\,\mathcal{L}_n(\lambda x) = \frac{\mathrm{d}^n}{\mathrm{d}a^n}\lambda^a\,\mathcal{L}^a(x)\Big|_{a=0} + \frac{\ln^{n+1}\lambda}{n+1}\delta(x) = \sum_{k=0}^{n}\binom{n}{k}\ln^k\lambda\,\mathcal{L}_{n-k}(x) + \frac{\ln^{n+1}\lambda}{n+1}\delta(x)\,. \tag{3.4}$$

where in this case, we take $\lambda = \frac{m\mu_\Gamma}{Q\mu_\Lambda}$.

The convolution is easier to execute in position space. Thus, we apply a Fourier transform to position space, compute the convolution, and then perform an inverse Fourier transform back to momentum space. To achieve this, we first shift $\hat{s}_t'$ and $\hat{s}_{\bar{t}}'$ to include $\hat{s}^+$ and $\hat{s}^-$,

$$\hat{s}_t' + \hat{s}^+ \to \hat{s}_t' \,, \tag{3.5}$$

$$\hat{s}_{\bar{t}}' + \hat{s}^+ \to \hat{s}_{\bar{t}}' \,, \tag{3.6}$$

and so our integral now has the form,

$$\int \mathrm{d}\hat{s}^{+} \int \mathrm{d}\hat{s}^{-} B_{+}\left(\hat{s}_{t}' - \hat{s}_{t}'' - \hat{s}^{+}\right) B_{-}\left(\hat{s}_{\bar{t}}' - \hat{s}_{\bar{t}}'' - \hat{s}^{-}\right) S(\hat{s}^{+}, \hat{s}^{-}) \,. \tag{3.7}$$

We apply the Fourier transform A.4 as follows

$$B_{+}\left(\hat{s}_{t}' - \hat{s}_{t}'' - \hat{s}^{+}\right) = \int \frac{\mathrm{d}y_{t}}{2\pi} e^{i(\hat{s}_{t}' - \hat{s}_{t}'' - \hat{s}^{+})y_{t}} \tilde{B}_{+}(y_{t}) \,, \tag{3.8}$$

$$B_{-}\left(\hat{s}_{\bar{t}}' - \hat{s}_{\bar{t}}'' - \hat{s}^{-}\right) = \int \frac{\mathrm{d}y_{\bar{t}}}{2\pi} e^{i(\hat{s}_{\bar{t}}' - \hat{s}_{\bar{t}}'' - \hat{s}^{-})y_{\bar{t}}} \tilde{B}_{-}(y_{\bar{t}}) \,, \tag{3.9}$$

Substituting these in the equation above, we get

$$\begin{aligned}
&\int \mathrm{d}\hat{s}^{+} \int \mathrm{d}\hat{s}^{-} \int \frac{\mathrm{d}y_{t}}{2\pi} e^{i(\hat{s}_{t}' - \hat{s}_{t}'' - \hat{s}^{+})y_{t}} \tilde{B}_{+}(y_{t}) \int \frac{\mathrm{d}y_{\bar{t}}}{2\pi} e^{i(\hat{s}_{\bar{t}}' - \hat{s}_{\bar{t}}'' - \hat{s}^{-})y_{\bar{t}}} \tilde{B}_{-}(y_{\bar{t}}) S(\hat{s}^{+}, \hat{s}^{-}) \\
&= \int \frac{\mathrm{d}y_{t}}{2\pi} \int \frac{\mathrm{d}y_{\bar{t}}}{2\pi} e^{i(\hat{s}_{t}' - \hat{s}_{t}'')y_{t}} e^{i(\hat{s}_{\bar{t}}' - \hat{s}_{\bar{t}}'')y_{\bar{t}}} \tilde{B}_{+}(y_{t}) \tilde{B}_{-}(y_{\bar{t}}) \times \int \mathrm{d}\hat{s}^{+} \int \mathrm{d}\hat{s}^{-} e^{-i\hat{s}_{t}^{+} y_{t}} e^{-i\hat{s}_{\bar{t}}^{-} t_{\bar{t}}} S\left(\hat{s}^{+}, \hat{s}^{-}\right) \,.
\end{aligned}$$

However,

$$\int \mathrm{d}\hat{s}^{+} \int \mathrm{d}\hat{s}^{-} e^{-i\hat{s}_{t}^{+} y_{t}} e^{-i\hat{s}_{\bar{t}}^{-} t_{\bar{t}}} S\left(\hat{s}^{+}, \hat{s}^{-}\right) = \tilde{S}\left(y_{t}, y_{\bar{t}}\right) \,, \tag{3.10}$$

so the above equation becomes

$$\int \frac{\mathrm{d}y_{t}}{2\pi} \int \frac{\mathrm{d}y_{\bar{t}}}{2\pi} e^{i(\hat{s}_{t}' - \hat{s}_{t}'')y_{t}} e^{i(\hat{s}_{\bar{t}}' - \hat{s}_{\bar{t}}'')y_{\bar{t}}} \tilde{B}_{+}(y_{t}) \tilde{B}_{-}(y_{\bar{t}}) \times \tilde{S}\left(y_{t}, y_{\bar{t}}\right) \,, \tag{3.11}$$

or

$$\mathrm{FT}\left[\tilde{B}_{+}(y_{t}) \tilde{B}_{-}(y_{\bar{t}}) \tilde{S}\left(y_{t}, y_{\bar{t}}\right)\right]\left(\hat{s}_{t}' - \hat{s}_{t}'', \hat{s}_{\bar{t}}' - \hat{s}_{\bar{t}}''\right) \,. \tag{3.12}$$

This allows us to simply multiply the series expansion of the $\tilde{B}$ and $\tilde{S}$ functions in the position space without having to deal with the complicated V_{k}^{mn} coefficients described in A.2. One can also write down a simple expression for the approximation of the non global part t_{2} in Eq. (2.18) in position space:

$$\tilde{t}_{2}(y_{t}, y_{\bar{t}}) = s_{ng}[0] + s_{ng}[2] \ln\left(\frac{y_{t}}{y_{\bar{t}}}\right)^{2} + s_{ng}[4] \ln\left(\frac{y_{t}}{y_{\bar{t}}}\right)^{4} + \ldots \,, \tag{3.13}$$

where the first few terms are

$$s_{ng}[0] = C_F T_F n_l \left(\frac{40}{81} + \frac{77\pi^2}{27} - \frac{52}{9}\zeta_3\right) + C_A C_F \left(-\frac{1070}{81} - \frac{871}{108}\pi^2 + \frac{7}{15}\pi^4 + \frac{143}{9}\zeta_3\right),$$
$$s_{ng}[2] = -C_F T_F n_l - C_A C_F \left(\frac{1}{2} + \frac{1}{3}\pi^2\right),$$
$$s_{ng}[4] = C_F T_F n_l \left(\frac{1}{108}\right) - C_A C_F \left(\frac{1}{27}\right). \tag{3.14}$$

We summarize the information above by defining $E_{\pm}^{\Gamma=0}$ such that

$$E_{\pm}^{\Gamma=0}\left(\hat{s}, \frac{Q}{m}, \mu_\Gamma, \mu_\Lambda\right) \equiv \int_{-\infty}^{\infty} \mathrm{d}l^{\pm} B_{\pm}\left(\hat{s} - \frac{Q}{m}, \Gamma_t = 0, \mu_\Gamma, \mu_\Lambda\right) S^{\text{part}}(l^{\pm}, \mu_\Lambda). \tag{3.15}$$

3.1.2 Including the Width

Now that we have combined the plus distributions in $B_{\pm}$ with those in S, we consider integration over the variable $\hat{s}''$. Note that this involves the BW, and so, the integrals take the form

$$\int_{-\infty}^{+\infty} \mathrm{d}s'' \frac{1}{\mu_\Gamma} \mathcal{L}_n\left(\frac{\hat{s}' - \hat{s}''}{\mu_\Gamma}\right) \frac{1}{\mu_\Lambda} \frac{\Gamma_t}{\pi(\hat{s}_t'^2 + \Gamma_t^2)}. \tag{3.16}$$

We define $\mathcal{E}$ such that

$$E_{\pm}^{\Gamma=0}\left(\hat{s}, \frac{Q}{m}, \mu_\Gamma, \mu_\Lambda\right) = \mathrm{Im}\left[\mathcal{E}_{\pm}^{\Gamma=0}\left(\hat{s}, \frac{Q}{m}, \mu_\Gamma, \mu_\Lambda\right)\right], \tag{3.17}$$

using the identity [30]

$$\mathrm{Im}\left[\frac{\ln^n(-x - i0)}{\pi(-x - i0)}\right] = \cos^2\left(\frac{n\pi}{2}\right) \frac{(-\pi^2)^{n/2}}{n+1}\delta(x) + \sum_{j=0}^{[[\frac{n-1}{2}]]} \frac{(-1)^j n! \pi^{2j}}{(2j+1)!(n-2j-1)!} \left[\frac{\theta(x)\ln^{n-2j-1}(x)}{x}\right]_+, \tag{3.18}$$

where $[[p]]$ on the sum is the greatest integer not exceeding p.

Thus, the general result of integration over $\hat{s}''$ takes the form

$$\int_{-\infty}^{+\infty} \mathrm{d}\hat{s}'' E_{\pm}^{\Gamma=0}\left(\hat{s}-\hat{s}'', \frac{Q}{m}, \mu_\Gamma, \mu_\Lambda\right) \frac{\Gamma_t}{\pi(\hat{s}''^2+\Gamma_t^2)} = \mathrm{Im}\left[\mathcal{E}_{\pm}^{\Gamma=0}\left(\hat{s}+i\Gamma_t, \frac{Q}{m}, \mu_\Gamma, \mu_\lambda\right)\right]. \tag{3.19}$$

Note that the integral is simple since it results in a shift of the invariant mass variable into the positive complex plane.

3.1.3 Including the Evolution

The final integration variable we consider is $\hat{s}'$. We must convolute the remaining terms with the evolution U_B. The relevant computations read

$$\int_{-\infty}^{+\infty} \mathrm{d}\hat{s}'\, U_B(\hat{s}-\hat{s}', \mu_\lambda, \mu_\Gamma) \frac{1}{\pi} \frac{\ln^n\left(\frac{-\hat{s}'-i\Gamma_t}{\mu_\Gamma}\right)}{\hat{s}+i\Gamma_t} \equiv -G_n(\hat{s}, \Gamma_t, \mu_\Lambda, \mu_\Gamma)\,, \tag{3.20}$$

where, from A.5,

$$G_n = \frac{1}{\pi}\mathrm{Im}\left[\frac{e^k(\mu_\Gamma e^{\gamma_E})^\omega \Gamma(1+\omega)}{(-\hat{s}-i\Gamma_t)^{1+\omega}} I_n\left(\frac{\hat{s}+i\Gamma_t}{\mu_\Gamma}, \omega\right)\right]. \tag{3.21}$$

Hence we see that the plus distributions turn into analytic functions when convoluted with the BW and evolution factors.

The result of these processes yield an equation of the form

$$\frac{\mathrm{d}\sigma^{\mathrm{part}}}{\mathrm{d}M_t^2\,\mathrm{d}M_{\bar{t}}^2} = \mathrm{d}\sigma^{\mathrm{part}} \sim \sum_{n=0}^{4}\sum_{m=0}^{4} c^{nm} G_n(\hat{s}_t, \Gamma_t, \mu_\Gamma, \mu_\Lambda) G_m(\hat{s}_{\bar{t}}, \Gamma_{\bar{t}}, \mu_\Gamma, \mu_\Lambda)\,. \tag{3.22}$$

This can be easily generalized for derivative terms that are induced by the subtractions. Using integration by parts the derivatives on B can be transformed in to overall derivatives of $\hat{s}_t$ and $\hat{s}_{\bar{t}}$. For example, for a mass subtraction term:

$$\begin{aligned} U_{B_+}(\hat{s}_t-\hat{s}_t')\left[\delta m_1(\mu)\frac{\mathrm{d}}{\mathrm{d}\hat{s}_t'}B_+\left(\hat{s}_t'-\frac{Q}{m}l^+-\hat{s}_t''\right)\right] S(l^+,l^-)\,\frac{1}{\pi}\frac{\Gamma_t}{(\hat{s}_t'')^2+\Gamma_t^2} \\ = \delta m_1 \frac{\mathrm{d}}{\mathrm{d}\hat{s}_t} U_{B_+}(\hat{s}_t-\hat{s}_t')\, B_+\left(\hat{s}_t'-\frac{Q}{m}l^+-\hat{s}_t''\right) S(l^+,l^-)\,, \end{aligned} \tag{3.23}$$

Similarly, since S contains derivative terms such as $\delta\Delta_{1,2}\left(\frac{\mathrm{d}}{\mathrm{d}l^+}+\frac{\mathrm{d}}{\mathrm{d}l^-}\right)S^{0,1}_{\mathrm{part}}(l^\pm,\mu)$, integration by parts yields terms of the form

$$B_+\left(\hat{s}_t-\frac{Q}{m}l^+,\mu\right)\frac{\mathrm{d}}{\mathrm{d}l^+}S^{0,1}(l^+,l^-)=\frac{Q}{m}\frac{\mathrm{d}}{\mathrm{d}\hat{s}_t}B_+\left(\hat{s}-\frac{Q}{m}l^+\right)S^{0,1}(l^+,l^-,\mu)\,. \quad (3.24)$$

3.2 Including the Model Function

The final integral remaining is that over the variables $\mathrm{d}\tilde{l}^\pm$. Including the combinations done above, our integral now takes the form

$$\frac{\mathrm{d}\sigma}{\mathrm{d}M_t^2\,\mathrm{d}M_{\bar{t}}^2}\propto\sum_{i,j}c^{i,j}\int\mathrm{d}\tilde{l}^+\,\mathrm{d}\tilde{l}^-G_i\left(\hat{s}_+-\frac{Q}{m}\tilde{l}^+\right)G_j\left(\hat{s}_--\frac{Q}{m}\tilde{l}^-\right)F(\tilde{l}^+,\tilde{l}^-)\,. \quad (3.25)$$

At this point, the code has achieved an analytic results for the G_i functions and the final $\tilde{l}^+$ and $\tilde{l}^-$ integration must be carried out numerically. Note that our definition of the model function from Eq. (2.21), reduces the problem to products of one dimensional integrals, such as

$$\int\mathrm{d}\tilde{l}^+G_i\left(\hat{s}_+-\frac{Q}{m}\tilde{l}^+\right)f_m\left(\frac{\tilde{l}^+}{\Lambda}\right)\times\int\mathrm{d}\tilde{l}^-G_j\left(\hat{s}_--\frac{Q}{m}\tilde{l}^-\right)f_n\left(\frac{\tilde{l}^-}{\Lambda}\right), \quad (3.26)$$

instead of complicated 2 dimensional integrals. These one dimensional integrals are carried our with standard GSL integrations packages available through SCETlib.

Chapter 4

Structure of the Code

The computations in this thesis were executed in C++ as part of a developing library called SCET-library (SCETlib). SCETlib is a C++ package for numerical calculations in QCD and SCET. Working in such a framework allowed us to borrow features universal to QCD and SCET, for example

- Running coupling for fixed number of flavors
- Anomalous dimensions $\gamma = \sum_{n=0}^{\infty} \gamma_n \left(\frac{\alpha}{4\pi}\right)^{n+1}$
- $\overline{\text{MS}}$ beta function for n_f fermions and general compact simple Lie group
- Constants such as C_F, C_A, T_f etc.

Moreover, the framework provides access to the GNU Scientific Library (GSL) [40], that allowed us to take advantage of predefined mathematical features such as

- Complex Numbers
- Integration
- Legendre Polynomials

This thesis contributed to the 'topjets' directory of SCETlib, which consisted of writing the files

- bHQETCoeffs: Encodes the coefficients of Eq. (2.11).

- MassScheme: Defines an enumeration type encoding the jet, pole and MSR scheme.
- MassSchemeCoeffs: Returns δm_1 and δm_2 according to the mass scheme.
- SCET_HardFunction: Encodes the function in Eq. (2.9).
- bHQET_HardFunction: Encodes the function in Eq. (2.10).
- ShemiCoeffs: Encodes Eq. (2.18).
- FourierTransform: Provides workspace to execute A.4.
- Evolution: Implements evolution of 1 and 2 dimensional series of plus functions with and without convolution with the BW. Also implements rescaling of plus functions.
- PFunctions: Combines all perturbative pieces of cross section, implements rescaling, evolution and renormalon corrections.
- Ifunc: Encodes the information in Eq. (A.14).
- CrossSection: Computes the cross section by combining the perturbative part with the model function.

Furthermore, some mathematical features of our own were implemented to contribute to the packages of SCETlib, specifically the Fourier Transform that was described in Section 3 and A.4. As an example, Fig. 4-1 highlights the code structure of the Pfunctions.

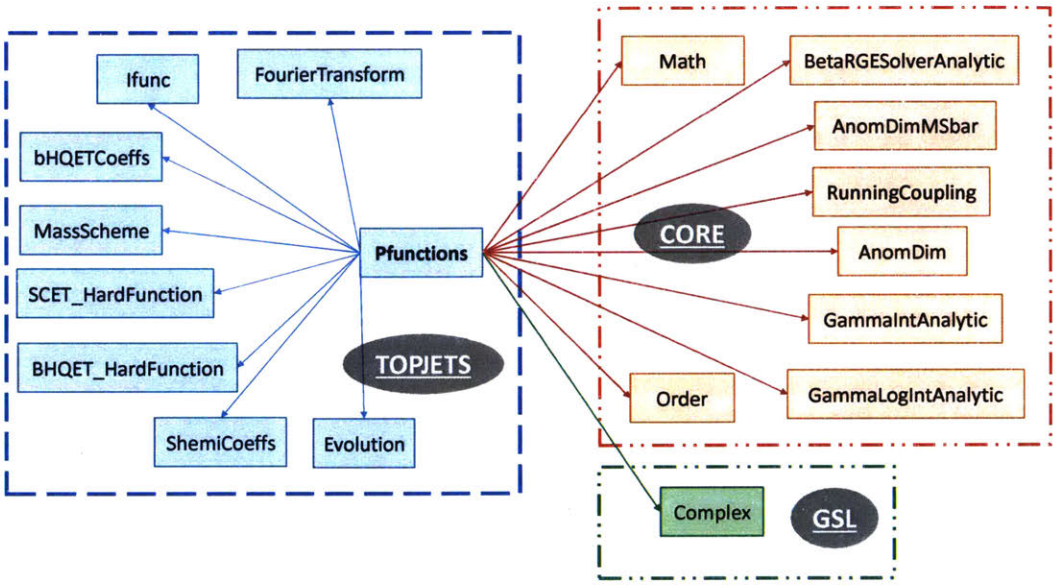

Figure 4-1: The Pfunctions are located in the topjets directory and depend on the other classes defined within topjets. The Pfunctions are able to access global SCETlib features defined in core, and are also capable of handling complex variables through GSL.

Chapter 5

Results

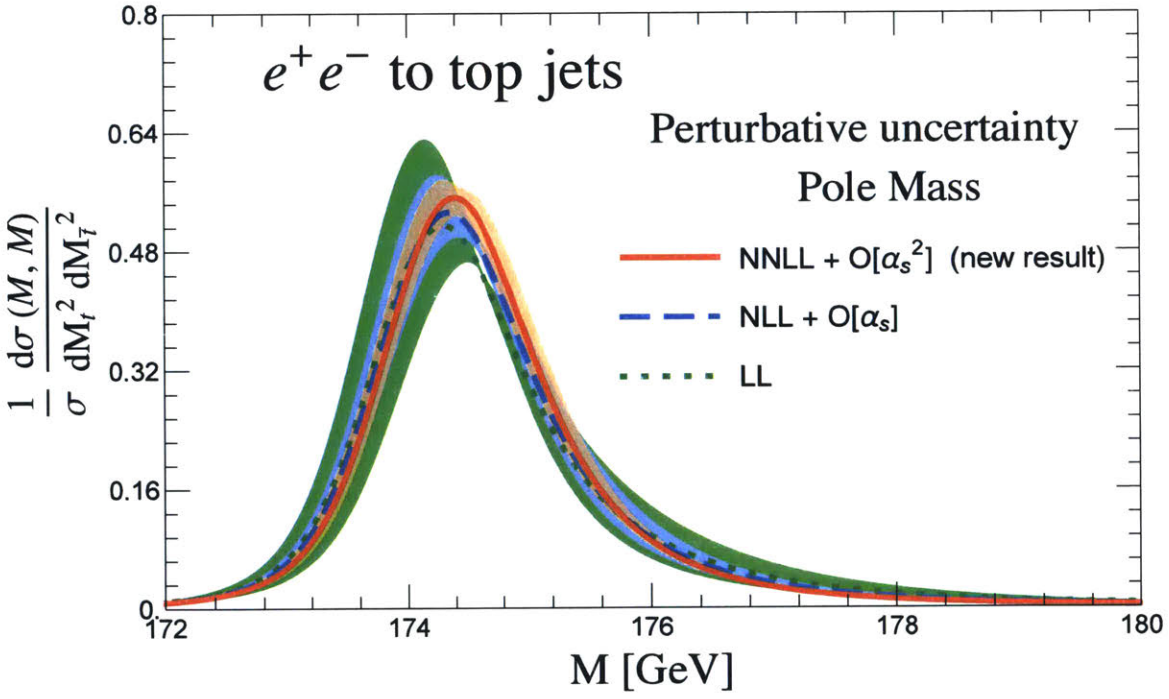

Figure 5-1: Perturbative convergence and uncertainty for the dijet invariant mass distribution.

In Fig. 5-1, we display the perturbative uncertainty of the normalized cross section at different orders for comparison. For simplicity we project the two dimensional distribution $\mathrm{d}\sigma^2/\,\mathrm{d}M_t^2\,\mathrm{d}M_{\bar{t}}^2$ along the diagonal with $M_t = M_{\bar{t}} = m$. We show our latest calculation NNLL′(=NNLL + $\mathcal{O}(\alpha_s^2)$ matrix elements) along with NLL′ and

LL results. The bands show at each order an estimate of perturbative uncertainty in the cross section due to the higher orders ignored in the calculation. This uncertainty is estimated by varying the various μ_i scales appearing in the cross section. The physical cross section does not depend on these renormalization scales, however, a calculation at a finite order in perturbation theory does vary with the μ_i scales and hence gives us a handle on estimating the uncertainty. We observe reduction of uncertainty as we go from LL to NLL′ to NNLL′ calculation. Furthermore, the fact that the bands are contained within each other shows convergence of perturbation theory.

The various renormalization scales that appear in the cross section are:

- μ_Λ : The soft scale $\sim \Lambda_{\rm QCD}$,
- μ_Γ : The jet function scale $\sim \Gamma_t$,
- μ_m : Scale for matching bHQET to SCET at m_t,
- μ_Q : Scale for matching SCET to QCD at Q.

The last two scales corresponding to the hard matching corrections, however, do not contribute to the uncertainty when we study normalized cross sections. These scales must take values consistent with the physics encoded by the corresponding functions. We noticed above that the convolution between the jet function and the soft function had the boost factor of Q/m. This produces logarithms of the form:

$$\ln\left(\frac{m\mu_\Gamma}{Q\mu_\Lambda}\right), \tag{5.1}$$

This implies that we should have a hierarchical relation between the μ_Γ and the μ_Λ scale of the form:

$$\mu_\Gamma \sim \mu_\Lambda \frac{Q}{m}, \tag{5.2}$$

in addition to the constraints listed above.

We also find that we have logs which have the form $\ln(\hat{s}_t/\mu_\Gamma)$. To minimize these logs we need make the μ scales dependent on the $\hat{s}_t$ parameter. The constraints that we listed above hold for the peak region, however, in the tail region we replace $\Gamma \to \hat{s}_t$ to obtain corresponding scaling. These $\hat{s}_t$ (or M_J) dependent scales are referred in the literature as profile functions. We follow the model of [41] to implement the profile scales. The uncertainty bands in Fig. 5-1 are generated from varying the profile scales about central values which satisfy the above constraints.

The plot shown in Fig. 5-1 contains pole mass as the input ($\delta m_i = 0$) and the renormalon corrections in the gap parameters have been also turned off ($\delta\Delta_i = 0$). In general there will be additional dependence from these renormalon subtraction parameters. These parameters are

- R_s : Scale for renormalon subtraction in the soft gap parameter,
- r : Scale for mass renormalon subtractions,

and the renormalization scales for evolution of these renormalon subtractions. The expected impact of these subtraction parameters is to improve the convergence for the peak location of Fig. 5-1 in going from LL$\to$NNL$' \to$ NNLL$'$ order. While these subtractions have been included in the code, at this time they have not been fully tested and calibrated. We leave exploration of constraints on these subtraction parameters, and associated uncertainties to future work.

Chapter 6

Conclusions

The reconstruction of the top quark invariant mass distribution is one of the major methods for measuring the top mass m at present and future colliders. Recent results of effective theory methods have presented an analytic factorization approach for the top invariant mass distribution in the peak region i.e. the double differential top/antitop invariant mass distribution $\mathrm{d}^2\sigma/\,\mathrm{d}M_t\,\mathrm{d}M_{\bar{t}}$ in e^+e^- collisions for center of mass energies $Q \gg m$, where $M_{t,\bar{t}}$ are defined as the total invariant masses of all the particles in the two hemispheres determined with respect to the event thrust axis.

In this thesis we use the results of EFTs to compute $\mathrm{d}^2\sigma/\,\mathrm{d}M_t\,\mathrm{d}M_{\bar{t}}$ to NNLL + NNLO, which goes beyond previous NLL+NLO analysis. We use the two-loop heavy quark jet-function, $\mathcal{O}(\alpha_s^2)$ corrections to the partonic hemisphere soft function, and hard matching for boosted tops at two loops. We execute this computation in SCETlib, to borrow already implemented features and also to develop new features for use by physicists in the future.

We observe convergence of perturbation theory of $\mathrm{d}^2\sigma/\,\mathrm{d}M_t\,\mathrm{d}M_{\bar{t}}$ as we go from LL$\to$NNL$'$ $\to$ NNLL$'$ order and also reduction of uncertainty, thus achieving the main goal of this calculation. Although this has been computed for the pole mass, the code contains the necessary ingredients implementing short distance mass schemes that are expected to improve convergence in the peak region going from LL$\to$NNL$'$ $\to$ NNLL$'$. In the future, we intend to extend the work presented here to include the analysis of these subtractions.

Appendix A

Background Formulas

A.1 Plus Distributions Definitions

The plus distributions are defined as

$$\mathcal{L}^a(x) = \left[\frac{\theta(x)}{x^{1-a}}\right] = \lim_{\epsilon\to 0}\frac{\mathrm{d}}{\mathrm{d}x}\left[\theta(x-\epsilon)\frac{x^a-1}{a}\right], \tag{A.1}$$

$$\mathcal{L}_n = \left[\frac{\theta(x)\ln^n x}{x}\right]_+ = \lim_{\epsilon\to 0}\frac{\mathrm{d}}{\mathrm{d}x}\left[\theta(x-\epsilon)\frac{\ln^{n+1} x}{n+1}\right], \tag{A.2}$$

$$\mathcal{L}_n^a(x) = \left[\frac{\theta(x)\ln^n x}{x^{1-a}}\right]_+ = \frac{\mathrm{d}^n}{\mathrm{d}b^n}\,\mathcal{L}^{a+b}(x)\Big|_{b=0}. \tag{A.3}$$

A.2 Convolution in momentum space

The convolutions of the plus distributions in momentum space can be achieved by [39],

$$\int \mathrm{d}y\,\mathcal{L}_m(x-y)\,\mathcal{L}_n(y) = \sum_{k=-1}^{m+n+1} V_k^{mn}\,\mathcal{L}_k(x) \tag{A.4}$$

$$\int \mathrm{d}y\,\mathcal{L}^a(x-y)\,\mathcal{L}_n(y) = \frac{1}{a}\sum_{k=-1}^{n+1} V_k^n(a)\,\mathcal{L}_k^a(x) - \frac{1}{a}\,\mathcal{L}_x(x) \tag{A.5}$$

where V_k^{mn} and $V_k^n(a)$ are defined as

$$V_k^{mn} = \begin{cases} \left.\frac{\mathrm{d}^m}{\mathrm{d}a^m}\frac{\mathrm{d}^n}{\mathrm{d}b^n}\frac{V(a,b)}{a+b}\right|_{a=b=0}, & \text{if } k=-1\,, \\ \left.\sum_{p=0}^{m}\sum_{q=0}^{n}\delta_{p+q,k}\binom{m}{p}\binom{n}{q}\frac{\mathrm{d}^{m-p}}{\mathrm{d}a^{m-p}}\frac{\mathrm{d}^{n-p}}{\mathrm{d}b^{n-q}}V(a,b)\right|_{a=b=0}, & \text{if } 0\le k\le m+n\,, \\ \frac{1}{m+1}+\frac{1}{n+1}\,, & \text{if } k=m+n+1\,. \end{cases} \tag{A.6}$$

$$V_k^n(a) = \begin{cases} \left.a\frac{\mathrm{d}^n}{\mathrm{d}b^n}\frac{V(a,b)}{a+b}\right|_{b=0]}, & \text{if } k=-1\,, \\ a\binom{n}{k}\frac{\mathrm{d}^{n-k}}{\mathrm{d}b^{n-k}}V(a,b)+\delta_{kn}\,, & \text{if } 0\le k\le n\,, \\ \frac{a}{n+1} & \text{if } k=n+1\,. \end{cases} \tag{A.7}$$

and

$$V(a,b) = \frac{\Gamma(a)\Gamma(b)}{\Gamma(a+b)} - \frac{1}{a} - \frac{1}{b}. \tag{A.8}$$

A.3 Rescaling Identity

$\mathcal{L}^a(x)$ satisfies the rescaling identity (for $\lambda > 0$) [39],

$$\lambda\,\mathcal{L}^a(\lambda x) = \lim_{\epsilon\to 0}\frac{\mathrm{d}}{\mathrm{d}x}\left[\theta(x-c)\frac{(\lambda x)^a-1}{a}\right] = \lambda^a\,\mathcal{L}^a(x) + \frac{\lambda^a-1}{a}\delta(x)\,, \tag{A.9}$$

from which we can obtain the rescaling identity

$$\lambda\,\mathcal{L}_n(\lambda x) = \left.\frac{\mathrm{d}^n}{\mathrm{d}a^n}\lambda^a\,\mathcal{L}^a(x)\right|_{a=0} + \frac{\ln^{n+1}\lambda}{n+1}\delta(x) = \sum_{k=0}^{n}\binom{n}{k}\ln^k\lambda\,\mathcal{L}_{n-k}(x) + \frac{\ln^{n+1}\lambda}{n+1}\delta(x)\,. \tag{A.10}$$

A.4 Fourier Transform

The Fourier transforms are defined as [31] (Position Space: $L_y = \ln(iye^{\gamma_E})$; y is dimensionless like the momentum space variable x).

Momentum to Position:

$$\begin{aligned}
\int \mathrm{d}t e^{-ity}\delta(t) &= 1 \\
\int \mathrm{d}t e^{-ity}\,\mathcal{L}_t^0 &= -L_y \\
\int \mathrm{d}t e^{-ity}\,\mathcal{L}_t^1 &= \frac{1}{2}L_y^2 + \frac{\pi^2}{12} \\
\int \mathrm{d}t e^{-ity}\,\mathcal{L}_t^2 &= -\frac{1}{3}L_y^3 - \frac{\pi^2}{6}L_y - \frac{2}{3}\zeta_3 \\
\int \mathrm{d}t e^{-ity}\,\mathcal{L}_t^3 &= \frac{1}{4}L_y^4 + \frac{\pi^2}{4}L_y^2 + 2\zeta_3 L_y + \frac{3}{80}\pi^4 .
\end{aligned} \tag{A.11}$$

Position to Momentum:

$$\begin{aligned}
\int \frac{\mathrm{d}y}{2\pi} e^{ity} &= \delta(t) \\
\int \frac{\mathrm{d}y}{2\pi} e^{ity} L_y &= -\,\mathcal{L}_t^0 \\
\int \frac{\mathrm{d}y}{2\pi} e^{ity} L_y^2 &= 2\,\mathcal{L}_t^1 - \frac{\pi^2}{6}\delta(t) \\
\int \frac{\mathrm{d}y}{2\pi} e^{ity} L_y^3 &= -3\,\mathcal{L}_t^2 + \frac{\pi^2}{2}\,\mathcal{L}_t^0 - 2\zeta_3\delta(t) \\
\int \frac{\mathrm{d}y}{2\pi} e^{ity} L_y^3 &= 4\,\mathcal{L}_t^3 - 2\pi^2\,\mathcal{L}_t^1 + 8\zeta_3\,\mathcal{L}_t^0 + \frac{\pi^4}{60} .
\end{aligned} \tag{A.12}$$

A.5 G Functions

The functions $G_n = G_n(\hat{s}, \Gamma_t, \mu_\Lambda, \mu_\Gamma)$ are defined as

$$G_n = \frac{1}{\pi}\mathrm{Im}\left[\frac{e^k(\mu_\Gamma e^{\gamma_E})^\omega \Gamma(1+\omega)}{(-\hat{s} - i\Gamma_t)^{1+\omega}} I_n\left(\frac{\hat{s} + i\Gamma_t}{\mu_\Gamma}, \omega\right)\right] . \tag{A.13}$$

Here $\omega = \omega(\mu_\Lambda, \mu_\Gamma)$ and $K = K(\mu_\Lambda, \mu_\Gamma)$, are described below [30] and

$$
\begin{aligned}
I_0(x,\omega) &= 1, \\
I_1(x,\omega) &= \ln(-xi0) - H(\omega), \\
I_2(x,\omega) &= [\ln(-x - i-) - H(\omega)]^2 + \psi^{(1)}(1+\omega) - \zeta_2, \\
I_3(x,\omega) &= [\ln(-x - i0) - H(\omega)]^3 + 3\left[\psi^{(1)}(1+\omega) - \zeta_2\right][\ln(-x - i0) - H(\omega)] \\
&\quad + \psi^{(2)}(1+\omega), \\
I_4(x,\omega) &= [\ln(-x - i0) - H(\omega)]^4 + 6\left[\psi^{(1)}(1+\omega) - \zeta_2\right][\ln(-x - i0) - H(\omega)]^2 \\
&\quad - 4\left[\psi^{(2)}(1+\omega) - \psi^{(2)}(1)\right][\ln(-x - i0) - H(\omega)] + \psi^{(3)}(1+\omega) - \psi^{(3)}(1) \\
&\quad + 3\left[\psi^{(1)}(1+\omega) - \zeta_2\right]^2,
\end{aligned}
\tag{A.14}
$$

with $H(\omega)$ the harmonic-number function, and $\psi^{(k)}(x)$ the kth derivative of the digamma function or equivalently the $(k+1)$th derivative of the log of the gamma function. Also the NNLL approximations of $\omega(\mu, \mu_0)$ and $K(\mu, \mu_0)$ are given by

$$
\begin{aligned}
\omega(\mu,\mu_0) &= -\frac{\Gamma_0^c}{\beta_0}\Bigg\{\ln(r) + \left(\frac{\Gamma_1^c}{\Gamma_0^c} - \frac{\beta_1}{\beta_0}\right)\frac{\alpha_s(\mu_0)}{4\pi}(r-1) \\
&\quad + \left(\frac{\Gamma_2^c}{\Gamma_0^c} - \frac{\beta_1\Gamma_1^c}{\beta_0\Gamma_0^c} - \frac{\beta_2}{\beta_0} + \frac{\beta_1^2}{\beta_0^2}\right)\frac{\alpha_s^2(\mu_0)}{32\pi^2}(r^2-1)\Bigg\}
\end{aligned}
\tag{A.15}
$$

$$
\begin{aligned}
K(\mu,\mu_0) &= \frac{-2\pi\Gamma_0^c}{\beta_0^2}\Bigg\{\frac{(r-1-r\ln r)}{r\alpha_s(\mu_0)} + \frac{\gamma_0\beta_0}{4\pi\Gamma_0^c}\ln r + \left(\frac{\Gamma_1^c}{\Gamma_0^c} - \frac{\beta_1^2}{\beta_0^2}\right)\frac{(1-r+\ln r)}{4\pi} \\
&\quad + \frac{\beta_1}{8\pi\beta_0}\ln^2 r + \frac{\alpha_s(\mu_0)}{16\pi^2}\Bigg[\frac{(\beta_0\gamma_1 - \beta_1\gamma_0)}{\Gamma_0^c}(r-1) + \left(\frac{\beta_1\Gamma_1^c}{\beta_0\Gamma_0^c} - \frac{\beta_2}{\beta_0}\right)(1-r+r\ln r) \\
&\quad + \left(\frac{\beta_2}{\beta_0} - \frac{\beta_1^2}{\beta_0^2}\right)(r-1)\ln r - \left(\frac{\Gamma_2^c}{\Gamma_0^c} - \frac{\beta_1\Gamma_1^c}{\beta_0\Gamma_0^c} - \frac{\beta_2}{\beta_0} + \frac{\beta_1^2}{\beta_0^2}\right)\frac{(1-r)^2}{2}\Bigg]\Bigg\}
\end{aligned}
\tag{A.16}
$$

Bibliography

[1] M. Kobayashi and T. Maskawa, "CP-Violation in the Renormalizable Theory of Weak Interaction," *Progress of Theoretical Physics*, vol. 49, pp. 652–657, Feb. 1973.

[2] S. Abachi *et al.*, "Observation of the top quark," *Phys. Rev. Lett.*, vol. 74, pp. 2632–2637, 1995.

[3] F. Abe *et al.*, "Observation of top quark production in $\bar{p}p$ collisions," *Phys. Rev. Lett.*, vol. 74, pp. 2626–2631, 1995.

[4] N. M. A. 2014, "The nobel prize in physics 2008," 2017.

[5] C. Patrignani *et al.*, "Review of Particle Physics," *Chin. Phys.*, vol. C40, no. 10, p. 100001, 2016.

[6] S. Heinemeyer, S. Kraml, W. Porod, and G. Weiglein, "Physics impact of a precise determination of the top quark mass at an e^+e^- linear collider," *JHEP*, vol. 09, p. 075, 2003.

[7] F. Bezrukov, M. Yu. Kalmykov, B. A. Kniehl, and M. Shaposhnikov, "Higgs Boson Mass and New Physics," *JHEP*, vol. 10, p. 140, 2012. [,275(2012)].

[8] J. Thaler and K. Van Tilburg, "Identifying Boosted Objects with N-subjettiness," *JHEP*, vol. 03, p. 015, 2011.

[9] J. Fan, P. Jaiswal, and S. C. Leung, "Jet Observables and Stops at 100 TeV Collider," 2017.

[10] G. Aad *et al.*, "Measurement of the top quark pair production charge asymmetry in proton-proton collisions at $\sqrt{s} = 7$ TeV using the ATLAS detector," *JHEP*, vol. 02, p. 107, 2014.

[11] V. Khachatryan *et al.*, "Search for resonant $t\bar{t}$ production in proton-proton collisions at $\sqrt{s} = 8$âĂĽâĂĽTeV," *Phys. Rev.*, vol. D93, no. 1, p. 012001, 2016.

[12] "First combination of Tevatron and LHC measurements of the top-quark mass," 2014.

[13] G. Cortiana, "Top-quark mass measurements: Review and perspectives," *Reviews in Physics*, vol. 1, pp. 60 – 76, 2016.

[14] F. Fiedler, A. Grohsjean, P. Haefner, and P. Schieferdecker, "The Matrix Element Method and its Application in Measurements of the Top Quark Mass," *Nucl. Instrum. Meth.*, vol. A624, pp. 203–218, 2010.

[15] J. Abdallah *et al.*, "Measurement of the Mass and Width of the W Boson in e^+e^- Collisions at $\sqrt{s}$ = 161-GeV - 209-GeV," *Eur. Phys. J.*, vol. C55, pp. 1–38, 2008.

[16] S. Fleming, A. H. Hoang, S. Mantry, and I. W. Stewart, "Jets from massive unstable particles: Top-mass determination," *Phys. Rev.*, vol. D77, p. 074010, 2008.

[17] A. H. Hoang and I. W. Stewart, "Top Mass Measurements from Jets and the Tevatron Top-Quark Mass," *Nucl. Phys. Proc. Suppl.*, vol. 185, pp. 220–226, 2008.

[18] V. S. Fadin and V. A. Khoze, "Production of a pair of heavy quarks in e+ e- annihilation in the threshold region," *Sov. J. Nucl. Phys.*, vol. 48, pp. 309–313, 1988. [Yad. Fiz.48,487(1988)].

[19] M. J. Strassler and M. E. Peskin, "Threshold production of heavy top quarks: Qcd and the higgs boson," *Phys. Rev. D*, vol. 43, pp. 1500–1514, Mar 1991.

[20] Y. Sumino, K. Fujii, K. Hagiwara, H. Murayama, and C.-K. Ng, "Top-quark pair production near threshold," *Phys. Rev. D*, vol. 47, pp. 56–81, Jan 1993.

[21] A. H. Hoang *et al.*, "Top - anti-top pair production close to threshold: Synopsis of recent NNLO results," *Eur. Phys. J.direct*, vol. 2, no. 1, p. 3, 2000.

[22] A. H. Hoang, A. V. Manohar, I. W. Stewart, and T. Teubner, "A Renormalization group improved calculation of top quark production near threshold," *Phys. Rev. Lett.*, vol. 86, pp. 1951–1954, 2001.

[23] A. H. Hoang, A. V. Manohar, I. W. Stewart, and T. Teubner, "The Threshold t anti-t cross-section at NNLL order," *Phys. Rev.*, vol. D65, p. 014014, 2002.

[24] M. Beneke *et al.*, "Top quark physics," in *1999 CERN Workshop on standard model physics (and more) at the LHC, CERN, Geneva, Switzerland, 25-26 May: Proceedings*, pp. 419–529, 2000.

[25] M. Butenschoen, B. Dehnadi, A. H. Hoang, V. Mateu, M. Preisser, and I. W. Stewart, "Top Quark Mass Calibration for Monte Carlo Event Generators," *Phys. Rev. Lett.*, vol. 117, no. 23, p. 232001, 2016.

[26] C. W. Bauer, S. Fleming, D. Pirjol, and I. W. Stewart, "An Effective field theory for collinear and soft gluons: Heavy to light decays," *Phys. Rev.*, vol. D63, p. 114020, 2001.

[27] T. Becher, A. Broggio, and A. Ferroglia, "Introduction to Soft-Collinear Effective Theory," *Lect. Notes Phys.*, vol. 896, pp. pp.1–206, 2015.

[28] S. Fleming, A. H. Hoang, S. Mantry, and I. W. Stewart, "Top Jets in the Peak Region: Factorization Analysis with NLL Resummation," *Phys. Rev.*, vol. D77, p. 114003, 2008.

[29] A. Manohar and M. Wise, *Heavy Quark Physics.* Cambridge Monographs on Partic, Cambridge University Press, 2007.

[30] A. Jain, I. Scimemi, and I. W. Stewart, "Two-loop Jet-Function and Jet-Mass for Top Quarks," *Phys. Rev.*, vol. D77, p. 094008, 2008.

[31] A. H. Hoang and S. Kluth, "Hemisphere Soft Function at $O(\alpha_s^2)$ for Dijet Production in e^+e^- Annihilation," 2008.

[32] A. Hornig, C. Lee, I. W. Stewart, J. R. Walsh, and S. Zuberi, "Non-global Structure of the $\mathcal{O}(\alpha_s^2)$ Dijet Soft Function," *JHEP*, vol. 08, p. 054, 2011.

[33] M. D. Schwartz, "Resummation and NLO matching of event shapes with effective field theory," *Phys. Rev.*, vol. D77, p. 014026, 2008.

[34] P. F. Monni, T. Gehrmann, and G. Luisoni, "Two-Loop Soft Corrections and Resummation of the Thrust Distribution in the Dijet Region," *JHEP*, vol. 08, p. 010, 2011.

[35] A. H. Hoang and I. W. Stewart, "Designing gapped soft functions for jet production," *Phys. Lett.*, vol. B660, pp. 483–493, 2008.

[36] T. Matsuura and W. L. van Neerven, "Second Order Logarithmic Corrections to the Drell-Yan Cross-section," *Z. Phys.*, vol. C38, p. 623, 1988.

[37] T. Matsuura, S. C. van der Marck, and W. L. van Neerven, "The calculation of the second order soft and virtual contributions to the Drell-Yan cross section," *Nuclear Physics B*, vol. 319, pp. 570–622, June 1989.

[38] A. H. Hoang, A. Pathak, P. Pietrulewicz, and I. W. Stewart, "Hard Matching for Boosted Tops at Two Loops," *JHEP*, vol. 12, p. 059, 2015.

[39] Z. Ligeti, I. W. Stewart, and F. J. Tackmann, "Treating the b quark distribution function with reliable uncertainties," *Phys. Rev.*, vol. D78, p. 114014, 2008.

[40] B. Gough, *GNU Scientific Library Reference Manual - Third Edition.* Network Theory Ltd., 3rd ed., 2009.

[41] A. H. Hoang, D. W. Kolodrubetz, V. Mateu, and I. W. Stewart, "Precise determination of α_s from the C-parameter distribution," *Phys. Rev.*, vol. D91, no. 9, p. 094018, 2015.